THE JOURNAL OF PHYSICAL CHEMISTRY B

Article

pubs.acs.org/JPCB

Toward a Rational Design of Bioactive Glasses with Optimal Structural Features: Composition–Structure Correlations Unveiled by Solid-State NMR and MD Simulations

Renny Mathew,[†] Baltzar Stevensson,[†] Antonio Tilocca,[‡] and Mattias Edén[†,*]

[†]Physical Chemistry Division, Department of Materials and Environmental Chemistry, Arrhenius Laboratory, Stockholm University, SE-106 91, Stockholm, Sweden

[‡]Department of Chemistry and Thomas Young Centre for the Theory and Simulations of Materials, University College London, London WC1H 0AJ, U.K.

Supporting Information

ABSTRACT: The physiological responses of silicate-based bioactive glasses (BGs) are known to depend critically on both the P content (n_P) of the glass and its silicate network connectivity ($\bar{N}^{Si}_{BO}$). However, while the bioactivity generally displays a nonmonotonic dependence on n_P itself, recent work suggest that it is merely the net orthophosphate content that directly links to the bioactivity. We exploit molecular dynamics (MD) simulations combined with ^{31}P and ^{29}Si solid-state nuclear magnetic resonance (NMR) spectroscopy to explore the quantitative relationships between $\bar{N}^{Si}_{BO}$, n_P, and the silicate and phosphate speciations in a series of $Na_2O-CaO-SiO_2-P_2O_5$ glasses spanning $2.1 \leq \bar{N}^{Si}_{BO} \leq 2.9$ and variable P_2O_5 contents up to 6.0 mol %. The fractional population of the orthophosphate groups remains independent of n_P at a fixed $\bar{N}^{Si}_{BO}$-value, but is reduced slightly as $\bar{N}^{Si}_{BO}$ increases. Nevertheless, P remains predominantly as readily released orthophosphate ions, whose content may be altered essentially independently of the network connectivity, thereby offering a route to optimize the glass bioactivity. We discuss the observed composition-structure links in relation to known composition-bioactivity correlations, and define how $Na_2O-CaO-SiO_2-P_2O_5$ compositions exhibiting an optimal bioactivity can be designed by simultaneously altering three key parameters: the silicate network connectivity, the (ortho)phosphate content, and the n_{Na}/n_{Ca} molar ratio.

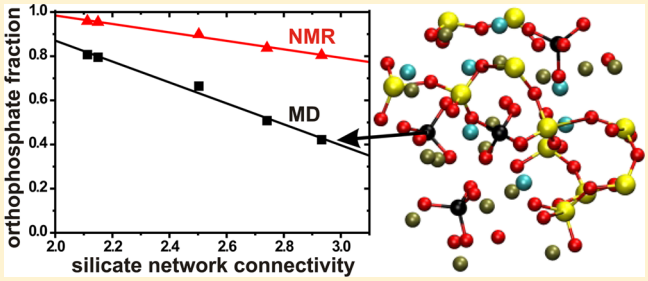

1. INTRODUCTION

Many melt-derived glasses of the $Na_2O-CaO-SiO_2-P_2O_5$ system, as well as other silicate-based analogues incorporating additional cations (e.g., Mg^{2+}, Sr^{2+}, Zn^{2+}) and/or anions (e.g., F^-) are termed "bioactive", as when subjected to body fluids, they spontaneously integrate with the tissue through a hydroxy-carbonate apatite (HCA) surface layer.[1−4] A few such *bioactive glass* (BG) options are widely exploited in orthopedic and periodontal surgery, e.g., the "45S5 Bioglass".[1−3]

Silicate-based glasses only exhibit bioactivity over a relatively narrow span of compositions. However, despite vast efforts being spent for improving and tailoring these materials, encompassing bioactivity assessments (i.e., the rate of HCA formation) both *in vitro* and *in vivo*,[2,3] very few quantitative composition/bioactivity relations are reported. The present insight thereof derives from empirical testing that typically involve systematic variations of the relative oxide contents, e.g., SiO_2 and P_2O_5.[2,3,5−9] Unfortunately, given the currently insufficient understanding of the underlying structure/composition relations that ultimately control the bioactivity, most empirically derived composition/bioactivity correlations have limited applicability to related BG formulations generated, for instance, by replacing glass modifier cations or by introducing additional glass network-forming elements, such as boron.

Considering the relatively modest progress made toward a rational design of BGs featuring optimal bioactivities via the relative oxide contents as direct variables, it is highly desirable to identify relatively simple descriptors[10] that reasonably accurately capture the essential composition/bioactivity relations through the insight provided from the underlying structure/composition links. Two such parameters are employed,[5,11,12] although relatively sparsely and not nearly to their full potential:

(i) One descriptor is the *silicate network connectivity*,[11−15] here denoted $\bar{N}^{Si}_{BO}$ and corresponding to the average number of bridging oxygen (BO) atoms per SiO_4 group in the structure. Q^n_{Si} labels a SiO_4 tetrahedron exhibiting n BO atoms and $4 - n$ nonbridging oxygen (NBO) ions. The negatively charged NBO species are balanced by the Na^+/Ca^{2+} modifiers. The importance of the network connectivity for the bioactivity was first highlighted by Strnad;[11] this concept was subsequently developed

Received: September 27, 2013
Revised: December 20, 2013
Published: December 23, 2013

   dx.doi.org/10.1021/jp409652k | J. Phys. Chem. B 2014, 118, 833−844

Table 1. BG Sample Compositions[a]

label	$\bar{N}^{Si}_{BO}$(nom)[b]	aNa$_2$O (mol %)	bCaO (mol %)	cSiO$_2$ (mol %)	dP$_2$O$_5$ (mol %)	stoichiometric formula	y(CaO)[c]	n_{Na}/n_{Ca}[d]	ρ (g cm^{-3})[e]
BG$_{2.6}$(2.1)	2.11	0.244 (0.229)	0.269 (0.255)	0.461 (0.486)	0.026 (0.030)	$Na_{0.384}Ca_{0.212}Si_{0.363}P_{0.041}O_{1.233}$	0.52	1.81	2.704
BG$_{6.0}$(2.1)	2.15	0.221 (0.207)	0.324 (0.315)	0.395 (0.412)	0.060 (0.065)	$Na_{0.345}Ca_{0.253}Si_{0.308}P_{0.094}O_{1.325}$	0.59	1.36	2.743
BG$_{0}$(2.5)	2.50	0.186 (0.178)	0.242 (0.231)	0.572 (0.591)	0.000 (0.000)	$Na_{0.314}Ca_{0.204}Si_{0.482}P_{0.000}O_{1.325}$	0.57	1.54	2.673
BG$_{1.0}$(2.5)	2.50	0.192 (0.181)	0.249 (0.250)	0.549 (0.559)	0.010 (0.010)	$Na_{0.319}Ca_{0.207}Si_{0.457}P_{0.017}O_{1.322}$	0.57	1.54	2.685
BG$_{2.0}$(2.5)	2.50	0.197 (0.191)	0.257 (0.258)	0.526 (0.527)	0.020 (0.024)	$Na_{0.324}Ca_{0.211}Si_{0.432}P_{0.033}O_{1.320}$	0.57	1.54	2.691
BG$_{4.0}$(2.5)	2.50	0.209 (0.193)	0.271 (0.254)	0.480 (0.509)	0.040 (0.044)	$Na_{0.334}Ca_{0.217}Si_{0.385}P_{0.064}O_{1.314}$	0.57	1.54	2.693
BG$_{6.0}$(2.5)	2.50	0.219 (0.201)	0.287 (0.274)	0.434 (0.460)	0.060 (0.065)	$Na_{0.343}Ca_{0.223}Si_{0.340}P_{0.094}O_{1.310}$	0.57	1.54	2.707
BG$_{2.6}$(2.7)	2.74	0.202 (0.194)	0.222 (0.214)	0.550 (0.560)	0.026 (0.032)	$Na_{0.329}Ca_{0.181}Si_{0.448}P_{0.042}O_{1.347}$	0.52	1.81	2.635
BG$_{0}$(2.9)	2.93	0.151 (0.143)	0.197 (0.183)	0.652 (0.674)	0.000 (0.000)	$Na_{0.262}Ca_{0.171}Si_{0.566}P_{0.000}O_{1.435}$	0.57	1.53	2.600
BG$_{2.0}$(2.9)	2.93	0.165 (0.151)	0.215 (0.206)	0.600 (0.623)	0.020 (0.020)	$Na_{0.278}Ca_{0.182}Si_{0.506}P_{0.034}O_{1.418}$	0.57	1.53	2.624
BG$_{3.0}$(2.9)	2.93	0.172 (0.161)	0.224 (0.226)	0.574 (0.583)	0.030 (0.030)	$Na_{0.286}Ca_{0.187}Si_{0.477}P_{0.050}O_{1.409}$	0.57	1.53	2.625
BG$_{4.0}$(2.9)	2.93	0.179 (0.162)	0.233 (0.226)	0.548 (0.572)	0.040 (0.040)	$Na_{0.294}Ca_{0.191}Si_{0.449}P_{0.066}O_{1.401}$	0.57	1.53	2.639
BG$_{6.0}$(2.9)	2.93	0.193 (0.172)	0.252 (0.244)	0.495 (0.524)	0.060 (0.060)	$Na_{0.308}Ca_{0.201}Si_{0.396}P_{0.096}O_{1.385}$	0.57	1.53	2.661

[a]{a, b, c, d} specify the nominally batched aNa$_2$O−bCaO−cSiO$_2$−dP$_2$O$_5$ oxide equivalents with $a + b + c + d = 1$; they were used for obtaining the stoichiometric formulae. Values within parentheses correspond to EDX-analyzed compositions. [b]The *silicate* network connectivity, i.e., average number of bridging oxygen atoms per SiO$_4$ tetrahedron, calculated by accounting for the modifier cation-consumption of the *ortho*phosphate species in each batched glass composition, according to the procedure of Edén.[15,23] [c]Molar fraction of CaO out of the glass modifier oxides; y(CaO) = n(CaO)/[n(CaO) + n(Na$_2$O)]. [d]Molar ratio between Na$^+$ and Ca^{2+} cations. [e]Densities (accurate within ±0.003 g cm^{-3}) were determined by the Archimedes method in water at 22 °C.

further and applied by several groups.[7,8,12,14−25] The exact limits of $\bar{N}^{Si}_{BO}$ required for bioactive glass compositions remain unsettled,[11,12,15,22] but "favorable" values are commensurate with open structures primarily built by Q^2_{Si} and Q^3_{Si} groups that readily degrade when subjected to body fluids.

(ii) The P content of the BG constitutes the second parameter for bioactivity predictions. Phosphorus is generally present as readily released *ortho*phosphate anions (i.e., Q^0_P groups) dispersed across the glass matrix.[26,27] Numerous investigations conducted both *in vitro* and *in vivo* reveal that the presence of P boosts the bioactivity.[2,3,5−7,9] Dissolved Ca^{2+} and PO_4^{3-} species increase the supersaturation of the HCA constituents in the body fluid, thereby accelerating the phosphate formation at the glass surface.[2,3,5,28] The ion release also controls the local pH and avoids excessive acidity that inhibits bone bonding.[29] However, if the glass-modifier content is insufficient for fully balancing all negative charges of the orthophosphate species, Q^1_P and higher-polymerization Q^n_P (n = 2, 3) phosphate moieties form. They are believed to diminish the bioactivity, owing to their lower mobility and the higher energetic cost associated with their release compared with the orthophosphate groups.[17,18] Yet, in *modifier-rich* BGs the existence and nature of the Q^1_P environments remains debated,[14−19,30−35] in particular which compositional/structural parameters control their populations.

Given that the glass bioactivity is enhanced either by a relatively low silicate network polymerization or by large amounts of orthophosphate groups, designing BGs that combine these two beneficial features is an appealing perspective for optimizing the bioactivity. One option involves adding P to a base glass composition, while the silicate network connectivity is kept fixed at a "favorable" value. However, any potential bearings on $\bar{N}^{Si}_{BO}$ or the Q^n_P speciation by introducing high P contents must first be assessed. The extent to which additional P atoms enter the silicate network and distribute between ortho- and nonorthophosphate moieties dictates if the goal indicated above is practically feasible, i.e., whether it is possible to design low-connectivity BGs that feature substantial orthophosphate contents. To answer this key question, herein we quantitatively examine the relationships between the phosphate speciation, the silicate network connectivity, and the P content of the glass across wide compositional ranges.

Herein, we assess the structural alterations accompanying the variations of the P content and $\bar{N}^{Si}_{BO}$ by monitoring the sets of $\{Q^n_{Si}\}$ and $\{Q^n_P\}$ populations that build each structure, as probed experimentally by magic-angle spinning (MAS) ^{29}Si and ^{31}P nuclear magnetic resonance (NMR) spectroscopy, as well as by molecular dynamics (MD) simulations.[36] The observed composition−structure correlations are linked with composition−bioactivity relationships reported in the literature to advance the structure−bioactivity insight; we further suggest rational ways to combine the key descriptors toward an optimal bioactivity. The present direct comparison between the MD and NMR derived structural features is also the first attempt of its kind for a large set of BG samples (*vide infra*), which further span a wide range of (Na, Ca, Si, P) compositions. Our results confirm that both experimental and computational approaches reveal fully consistent qualitative trends. This mutual validation is also important for enabling discussions on specific MD-derived structural features that are not experimentally accessible.[36]

2. GLASS SERIES DESIGN

To elucidate the structural changes resulting from variations of *either* the P content *or* the silicate network connectivity while the other parameter remains fixed, we prepared a set of 13 BG specimens from the quaternary Na$_2$O−CaO−SiO$_2$−P$_2$O$_5$ system, each labeled BG$_p$($\bar{N}^{Si}_{BO}$), with $0 \le p \le 6.0$ representing the P$_2$O$_5$ content in mol % (see Table 1). Two glass series featuring *nominal* $\bar{N}^{Si}_{BO}$ values of $\bar{N}^{Si}_{BO}$(nom)=2.5 and $\bar{N}^{Si}_{BO}$(nom)=2.9, respectively, were derived by *assuming* that P is present solely as *ortho*phosphate groups (Q^0_P) in each glass structure, thereby requiring a known net amount of the Na$^+$/Ca^{2+} network modifiers for charge balance. Both BG

dx.doi.org/10.1021/jp409652k | J. Phys. Chem. B 2014, 118, 833−844

families exhibit a constant molar ratio n_{Na}/n_{Ca} = 1.54, and the modifier reservoir consistently remains sufficiently large for simultaneously arranging the desired $\bar{N}^{Si}_{BO}$-value together with the sole presence of Q^0_P groups. This BG design strategy, employed in a few recent studies,[14,22,31] implies that the total $n_{Na}+n_{Ca}$ amount increases concurrently with n_P across each BG(2.5) and BG(2.9) series, while that of Si decreases, *approximately* amounting to a net Si→P stoichiometric replacement (see Table 1).

Besides each BG(2.5) and BG(2.9) branch (where we drop the *p* subscript when collectively referring to all its members), two additional samples—$BG_{2.6}(2.1)$ and $BG_{2.6}(2.7)$—form a set of glasses exhibiting roughly constant P_2O_5 contents (2−3 mol %), but with $\bar{N}^{Si}_{BO}$ increasing from 2.1 to 2.9. This series enables us to selectively probe the structural changes resulting when *solely* the silicate network-connectivity varies. Note that the $BG_{2.6}(2.1)$ specimen corresponds to the widely utilized "45S5 Bioglass".[1−3]

The primary aim of the present work is to enhance the structure−bioactivity insight by exploring the phosphate and silicate speciations of both bioactive and nonbioactive glass compositions that are selected based on the following *hypotheses*, inferred and discussed by Edén[15] on the basis of *in vitro* bioactivity tests reported in the literature:[6,7] (**A**) A *silicate* network connectivity conforming to the range $2.0 \lesssim \bar{N}^{Si}_{BO} \lesssim 2.7$ is a prerequisite for bioactivity; it is optimized for values around 2.5−2.6.[15] (**B**) Provided that requirement **A** is fulfilled, the bioactivity grows monotonically with the net *ortho*phosphate content

$$n^0_P = x^0_P n_P \quad (1)$$

where n_P is the stoichiometric amount of P (see Table 1). Here and onward, x^n_P and x^n_{Si} denote the fractional population of Q^n_P and Q^n_{Si} groups out of the total $\{Q^n_P\}$ and $\{Q^n_{Si}\}$ speciation, respectively. In this work, we examine and discuss hypotheses **A** and **B** further.

3. MATERIALS AND METHODS

3.1. Sample Preparations and Characterization. The BGs were prepared from precursors of NaH_2PO_4 (99.99%; Merck), and Na_2CO_3 (99.9%), $CaCO_3$ (99.9%), and SiO_2 (99.99%) from ChemPur. To accelerate spin−lattice relaxation for the NMR experimentation, 0.1 wt % of Fe_2O_3 was added to each batch. Each precursor-mixture (6.0 g) was ball-milled for 12 h and subsequently placed in a Pt crucible that was heated for 4 h in an electric furnace at 950 °C for CO_2 removal. The temperature was set to a final value in the range of 1350−1620 °C, with the highest temperatures required by compositions exhibiting a large P-content and/or high $\bar{N}^{Si}_{BO}$-value. Each melt was held for 4 h prior to its quenching by immersing the bottom of the crucible in water.

Powder X-ray diffraction with a PANalytical X'pert PRO MPD diffractometer and Cu $K\alpha_1$ radiation revealed no crystalline phases (detection limit $\lesssim$1%). Here, 2θ ranged between 10° and 70°. Scanning electron microscopy (SEM) with a JSM 7000F (JEOL) microscope in backscatter electron imaging mode (20 kV acceleration voltage) evidenced that each specimen constitutes a homogeneous glass phase, except for $BG_{6.0}(2.9)$ that manifested tendencies of amorphous phase-separation. Cation contents were estimated by a LINK INCA (Oxford instruments) energy-dispersive X-ray (EDX) detector. Each reported composition resulted from averaging over ten analyses from distinct fragments, with the respective O content calculated to charge-balance the cations. The nominal and EDX-analyzed glass compositions agree overall well (see Table 1), where the deviations remain within the uncertainty of the analysis. Hence, the sample nomenclature and structural analysis assume the nominal glass compositions. See Mathew et al.[25] for further synthesis/characterization details.

3.2. Solid-State NMR Experiments. All MAS NMR experimentation utilized a Bruker Avance-III spectrometer operating at 9.4 T; i.e., the ^{31}P and ^{29}Si Larmor frequencies are −162.0 MHz and 79.47 MHz, respectively. Finely ground glass powders were packed in 7 mm zirconia rotors and spun at 7.00 kHz. The NMR acquisitions utilized single pulses with flip angles, rf nutation frequencies, and relaxation delays of {70°, 62.5 kHz, 120 s} and {90°, 81 kHz, 40 s} for ^{29}Si and ^{31}P, respectively, with the corresponding number of accumulated signal transients depending on the content of the detected nucleus and ranging over 400−900 and 256−640. Separate T_1 relaxation measurements verified that these relaxation delays provide quantitative NMR spectra. No signal apodization was employed in the data processing. ^{31}P and ^{29}Si chemical shifts are quoted relative to 85% H_3PO_4(aq) and neat tetramethylsilane (TMS), respectively.

3.3. Molecular Dynamics Simulations. Classical MD simulations were performed with the DLPOLY3 package[37,38] for *NVT* ensembles, where 6000−12000 {Na, Ca, Si, P, O} atoms were placed in a cubic box with periodic boundary conditions and a size within 4.2−5.1 nm; these numbers varied slightly to match each nominal BG composition and experimental density (see Table 1 and the Supporting Information). The melt-quench simulation started from a random atom configuration, equilibrated for 100 ps at 3500 K, followed by a 10 K/ps cooling procedure down to 300 K. A final *NVT* run at 300 K was then performed for 200 ps, of which the last 150 ps were used for the structural analysis. For each glass composition, this protocol was completed 2−4 times with different initial configurations (see the Supporting Information). The average value and uncertainty of each reported structural parameter were derived from these independent samples.

A polarizable shell-model potential, developed for modeling multicomponent glasses,[17−19,39] was employed throughout. Each cation carries its full formal charge. O^{2-} species are represented as core (O_C) and shell (O_S) units coupled by a 300 THz harmonic oscillator and bearing charges of z_C = 0.8482*e* and z_S = −2.8482*e*, respectively (i.e., $z_C + z_S = -2e$ constitutes the formal charge). The short-range O_S-O_S and cation−O_S interactions were parametrized by a Buckingham potential,[17−19,39] evaluated for all pairs up to 0.8 nm. Long-range Coulombic interactions among all charged particles were calculated by a smoothed particle mesh Ewald summation[38] with a 1.2 nm real-space cutoff and an accuracy of 10^{-6}. The intratetrahedral O−Si−O and O−P−O bond angles were constrained by using three-body truncated harmonic potentials.[38] The equations of motion were integrated in time-steps of 0.2 fs by the velocity Verlet integrator approach. The temperature was controlled by a Berendsen thermostat with a 1.0 ps relaxation time constant. See refs 17−19 and 39 for further details on the simulation procedures, and the Supporting Information for additional discussions on the convergence of the MD data with respect to the system size and the cooling rate of the simulation.

4. RESULTS

4.1. ^{31}P NMR. The ^{31}P MAS NMR spectra recorded from the BG(2.5) and BG(2.9) series are displayed in Figure 1.

dx.doi.org/10.1021/jp409652k | J. Phys. Chem. B 2014, 118, 833−844

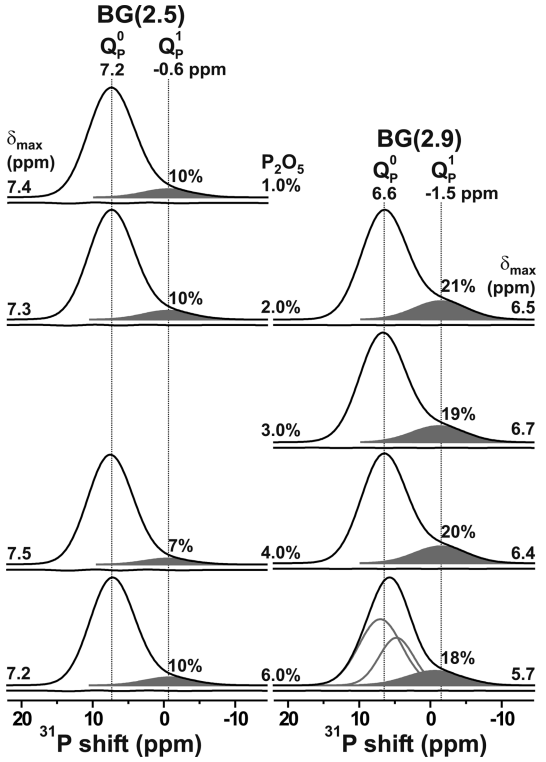

Figure 1. Experimental ^{31}P MAS NMR spectra recorded from Na_2O–CaO–SiO_2–P_2O_5 glasses, where the BG(2.5) and BG(2.9) series are displayed in the left and right columns, respectively, and ordered according to increasing P_2O_5 contents from top to bottom. The peak maximum is specified at the outermost portion of each spectrum; it is mainly dictated by the ^{31}P resonances from Q_P^0 groups, whose traces are not indicated, except for the NMR spectrum from $BG_{6.0}(2.9)$ that required deconvolutions into two distinct ^{31}P signals. Shaded areas mark signal contributions from Q_P^1 moieties, whose relative populations (in %) are indicated. The curve beneath each spectrum reveals the difference between the experimental and best-fit spectra.

All are representative of phosphate groups in strongly disordered structures, as reflected by NMR signals associated with 7.5–8.0 ppm full-width at half-maximum (fwhm) height. Onward disregarding the $BG_{6.0}(2.9)$ sample that is not fully homogeneous (see section 3.1), all specimens within each fixed-$\bar{N}_{BO}^{Si}$ series exhibit essentially equal ^{31}P NMR peak maxima (δ_{max}) and fwhm values, regardless of the P content. The observed peak maxima in the range 6–9 ppm are consistent with Q_P^0 (orthophosphate) environments charge-balanced by both Na^+ and Ca^{2+}.[26,27,40]

The NMR peakshape recorded from each BG(2.5) glass is nearly Gaussian, but it becomes progressively more asymmetric when the silicate-network connectivity increases: this growing "tail" stems from Q_P^1 groups.[16,20,25−27,31−33,41,42] A main goal of the present work is to quantify these populations and rationalize their dependence on the silicate network connectivity and P content of the BG. The Supporting Information discusses the problems of detecting low amounts of Q_P^1 groups by solid-state ^{31}P NMR on BGs (such as the most thoroughly studied "45S5" composition; e.g., see Pedone et al.[30]), as well as highlighting their assisted probing by exploiting information from the spinning sidebands in the NMR spectrum. While we for brevity denote the $n \geq 1$ phosphate moieties by Q_P^n, their BO atoms all involve linkages to Si rather than P, as highlighted previously in numerous MD studies,[17−19,30] as well as experimentally by through-space and through-bond coupling-based NMR techniques.[33,41] We note that standard ^{31}P MAS NMR experimentation cannot discriminate between ^{31}P in Si–O–P and P–O–P motifs.[33,41] The MD-derived fractions of P–O–P bonds in the present glasses remain very low ($\lesssim$ 3% out of all P–O–Si and P–O–P motifs) and are only present in the P-richest samples featuring ≥4 mol % P_2O_5.

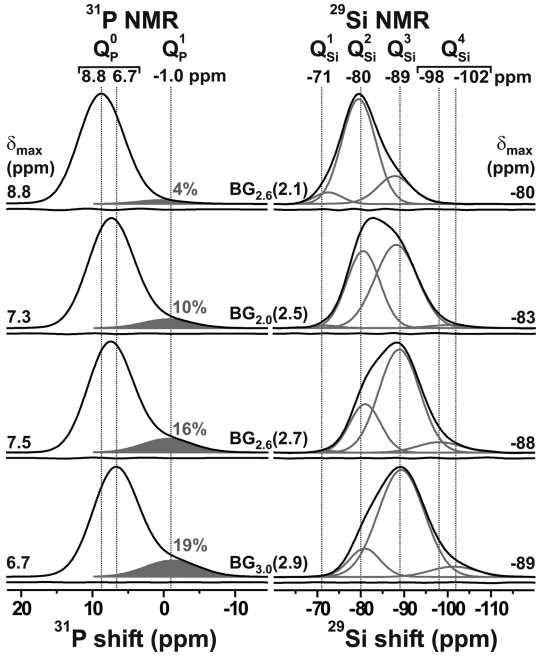

Figure 2. Experimental ^{31}P (left column) and ^{29}Si (right column) NMR spectra, plotted with black traces and acquired from the as-indicated $BG_p(\bar{N}_{BO}^{Si})$ samples. The spectra are listed according to increasing silicate network connectivity from top to bottom. Each ^{31}P NMR contribution from the Q_P^1 groups is marked by a shaded area (left column), with the respective population (in %) specified. The gray traces in the right column represent ^{29}Si NMR peaks stemming from the various Q_{Si}^n groups, as obtained by spectral deconvolution. The curve beneath each NMR spectrum represents the difference between the experiment and its respective best-fit.

The ^{31}P NMR results of Figure 2 from glasses featuring a nearly constant P content (2–3 mol % P_2O_5) but variable $\bar{N}_{BO}^{Si}$ values between 2.1 and 2.9, suggest a strict relationship between the fraction of Q_P^1 groups in the BG structure and its silicate network connectivity. To quantify these relationships further, we deconvoluted each ^{31}P NMR signal into two Gaussian peak components stemming from Q_P^0 and Q_P^1 species by constrained iterative fitting (see the Supporting Information). Each peak is represented by the parameter-triplet (δ_P^n, W_P^n, x_P^n), corresponding to the mean ^{31}P chemical shift, the fwhm, and the fractional population, respectively, of the given Q_P^n species. The best-fit results are listed in Table 2. They reveal no significant variations across the set of BGs, as anticipated from the very similar experimental ^{31}P NMR spectra. Owing to the higher ^{31}P shielding resulting from $Q^n \rightarrow Q^{n+1}$ conversions, the chemical shifts associated with Q_P^0 and Q_P^1 groups are separated by ≈8 ppm, with those from Q_P^0 moieties appearing within a narrow window of 6.4–8.7 ppm, whereas their Q_P^1 counterparts span between −1.7 ppm and 0.4 ppm. As discussed further in section 4.3, the results from BGs associated with four distinct $\bar{N}_{BO}^{Si}$-values evidence a concurrent growth of

dx.doi.org/10.1021/jp409652k | J. Phys. Chem. B 2014, 118, 833−844

Table 2. ^{31}P NMR Results[a]

	net peak		Q_P^0			Q_P^1				
label	δ_{max} (ppm)	W (ppm)	δ^0 (ppm)	W^0 (ppm)	x^0	δ^1 (ppm)	W^1 (ppm)	x^1	$\bar{N}_{BO}^{Si}$(nom)	$\bar{N}_{BO}^{Si}$(NMR$_P$)[b]
$BG_{2.6}$(2.1)	8.8	7.51	8.7	7.4	0.959	0.4	7.3	0.041	2.11	2.11
$BG_{6.0}$(2.1)	7.3	7.48	7.3	7.4	0.955	−0.8	7.4	0.045	2.15	2.14
BG_0(2.5)	–	–	–	–	–	–	–	–	2.50	2.50
$BG_{1.0}$(2.5)	7.4	7.77	7.4	7.6	0.899	−0.6	8.1	0.101	2.50	2.50
$BG_{2.0}$(2.5)	7.3	7.72	7.4	7.5	0.896	−0.6	8.3	0.104	2.50	2.50
$BG_{4.0}$(2.5)	7.5	7.57	7.5	7.4	0.931	−0.6	7.9	0.069	2.50	2.49
$BG_{6.0}$(2.5)	7.2	7.55	7.2	7.4	0.902	−0.8	8.2	0.098	2.50	2.48
$BG_{2.6}$(2.7)	7.5	7.72	7.5	7.4	0.838	−0.6	8.4	0.162	2.74	2.73
BG_0(2.9)	–	–	–	–	–	–	–	–	2.93	2.93
$BG_{2.0}$(2.9)	6.5	7.96	6.4	7.5	0.795	−1.7	8.6	0.205	2.93	2.92
$BG_{3.0}$(2.9)	6.7	7.97	6.8	7.5	0.814	−1.2	8.9	0.186	2.93	2.91
$BG_{4.0}$(2.9)	6.4	7.85	6.5	7.4	0.805	−1.5	8.7	0.195	2.93	2.90
$BG_{6.0}$(2.9)[c]	5.7	7.47	7.0	7.1	0.549	−0.6	9.2	0.179	2.93	2.89
			4.8	5.7	0.272					

[a]The data involves the net NMR chemical shift (δ_{max}; uncertainty ±0.1 ppm) and fwhm height (W; ±0.15 ppm) of the ^{31}P NMR signal, as well as the chemical shift (δ^n; ±0.3 ppm), fwhm height (W^n; ±0.5 ppm), and fractional population (x^n; ±0.02) of each Q_P^n contribution extracted by spectra deconvolution. [b]Vaules corrected for the NMR-derived minor Q_P^1 contributions. [c]This sample exhibits phase separation and its ^{31}P NMR spectrum required two Q_P^0 signals for deconvolution.

the relative fraction of the Q_P^1 environments from ≈0.05 to ≈0.20 when $\bar{N}_{BO}^{Si}$ is increased between 2.1 and 2.9, whereas the x_P^1 values are independent of the P content within each BG($\bar{N}_{BO}^{Si}$) series.

For a fixed number of NBO ions at the phosphate group, its ^{31}P chemical shift is dictated mainly by the nature and location of the surrounding glass-modifier cations.[16,27,31,40] Previous ^{31}P NMR reports on Na−Ca−Si−P−O glasses[16,25,27,30−32,43] observed δ_P^0 values that are intermediate of the shifts associated with the orthophosphate groups present in polymorphs of Na_3PO_4 and $Ca_3(PO_4)_2$ that resonate around 12−15 ppm and 0−3 ppm, respectively. A linear relationship between δ_P^0 and $y(CaO) = n(CaO)/[n(CaO) + n(Na_2O)]$ is reported for $Na_2O-CaO-SiO_2-P_2O_5$ glasses.[16,27,31] The present ^{31}P NMR results for BGs featuring a nearly *constant* y(CaO) value accord with those findings: the following weighted average,

$$\bar{\delta}_P^0 = y(CaO)\delta_A + [1 - y(CaO)]\delta_B \quad (2)$$

with y(CaO) = 0.57 for the BG(2.5) and BG(2.9) series (see Table 1), predicts a chemical-shift range of $5.2 \leq (\bar{\delta}_P^0/\text{ppm}) \leq 8.2$ for the Q_P^0 groups when δ_A and δ_B are selected over the typical shift-spans of crystalline Na and Ca based orthophosphates, i.e., 12−15 ppm and 0−3 ppm, respectively. Consequently, our observed δ_P^0 values in the range of 6.5−7.5 ppm are overall consistent with earlier NMR work reporting an essentially statistical Na/Ca distribution around the orthophosphate species;[16,27,31,43] see the Supporting Information for further discussions.

The present NMR analysis cannot discriminate between a *strict* statistical (Na,Ca)−P association and minor preferences of either cation to charge-balance the phosphate moieties. A more accurate ^{17}O NMR analysis applied to the 45S5 BG, revealed a slight depletion of $Na^+-PO_4^{3-}$ contacts,[30] while previous MD simulations also suggested a strong preference for $Ca^{2+}-PO_4^{3-}$ rather than $Na^+-PO_4^{3-}$ associations,[17,44−46] as also observed in our modeled $BG_{2.6}$(2.1) structure. The MD-derived Na/Ca partitioning among Si/P for the entire glass series will be presented together with those from a more extended NMR study in a forthcoming paper.

4.2. ^{29}Si NMR. For Na−Ca−Si−P−O glasses, the mean ^{29}Si chemical shift (δ_{Si}^n) of a Q_{Si}^n species depends principally on the same structural factors as ^{31}P, i.e., the number of BO atoms (n) at the SiO_4 tetrahedron, and the Na^+/Ca^{2+} constellation for local charge-balance.[16,27,40,47,48] All glasses within a given BG($\bar{N}_{BO}^{Si}$) branch exhibit a constant n_{Na}/n_{Ca} ratio. Consequently, the center-of-gravity shift (δ_{CG}) of the ^{29}Si NMR peak and the accompanying peakshape are expected to depend predominantly on the precise set of fractional populations $\{x_{Si}^n\}$ and their associated $\{\delta_{Si}^n\}$ values, where ^{29}Si nuclei of Q_{Si}^4 moieties typically resonate in the range from −112 ppm to −100 ppm and the shift increases by roughly 7−12 ppm per $Q_{Si}^n \rightarrow Q_{Si}^{n-1}$ conversion.[40,47,48] Hence, for the present glasses, identical ^{29}Si NMR responses are expected throughout a given BG($\bar{N}_{BO}^{Si}$) series, whereas a gradual net displacement toward more negative shifts should occur when $\bar{N}_{BO}^{Si}$ increases. The latter trend is witnessed by the ^{29}Si MAS NMR spectra presented in Figure 2. In contrast, very similar spectra are observed across each BG(2.5) and BG(2.9) branch, regardless of the P content of the BG; see the top row of Figure 3. Furthermore, Table 3 reveals very similar sets of ^{29}Si NMR best-fit parameters $\{\delta_{Si}^n, W_{Si}^n, x_{Si}^n\}$ within each $\bar{N}_{BO}^{Si}$-branch.

The net NMR responses derive from superimposed signals centered at the chemical shifts $\{\delta_{Si}^4, \delta_{Si}^3, \delta_{Si}^2, \delta_{Si}^1\}$ that appear around {−101, −88, −81, −72} ppm, respectively (see Figures 2 and 3). However, typically only three components are significant across the entire $\bar{N}_{BO}^{Si}$-span of the present glasses, of which two moieties dominate: Q_{Si}^2 and Q_{Si}^3. The networks of the BG(2.9) glasses are primarily built by Q_{Si}^3 groups (≈78% out of the total SiO_4 speciation), as expected, with the remaining constituting roughly equal amounts ≈10% of Q_{Si}^4 and Q_{Si}^2 groups. While minor Q_{Si}^2 contributions *must* be present because $\bar{N}_{BO}^{Si} < 3.0$, the NMR spectra unambiguously also reveal the presence of Q_{Si}^4 groups. This feature stems from disproportionation equilibria, such as $2Q_{Si}^n \leftrightarrow Q_{Si}^{n+1} +$

dx.doi.org/10.1021/jp409652k | J. Phys. Chem. B 2014, 118, 833−844

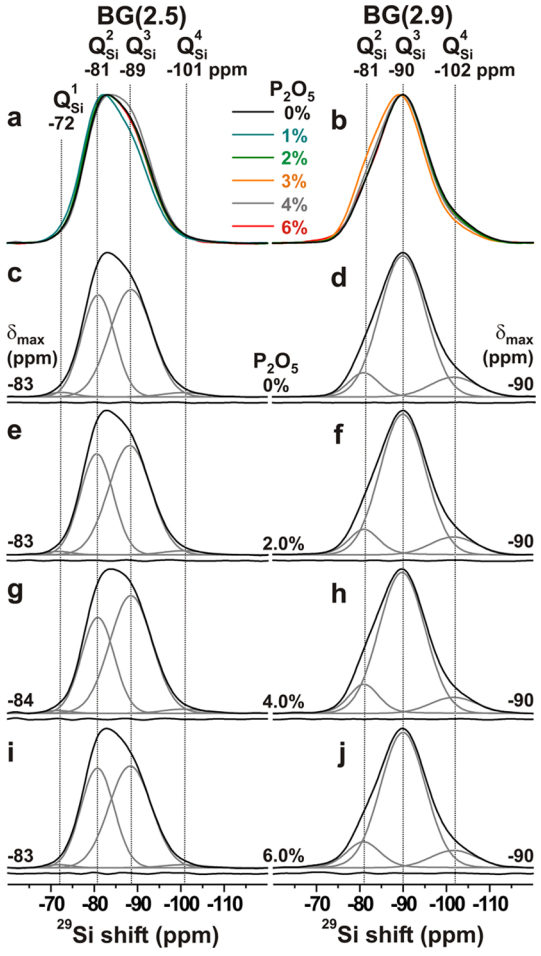

Figure 3. ^{29}Si MAS NMR spectra obtained from the BG(2.5) (left column) and BG(2.9) (right column) series of glasses. (a, b) Superimposed NMR spectra associated with the as-indicated glasses. (c–j) Experimental spectra (black traces) displayed together with deconvoluted peak-components (gray traces). They are assigned at the top of each column. The curves beneath the spectra constitute differences between experiments and best-fits.

Q^{n-1}_{Si}.[40,47,48] They produce deviations from a strict *binary* distribution that predicts the coexistence of only two tetrahedral species, Q^n_{Si} and Q^{n+1}_{Si}, except when $\bar{N}^{Si}_{BO}$ equals any member of the set {0, 1, 2, 3, 4}, when one sole Q^n_{Si} group associated with $n = \bar{N}^{Si}_{BO}$ results. A similar trend is observed for the BG(2.5) series for which a binary distribution predicts equal $\{x^2_{Si}, x^3_{Si}\}$ values, whereas the NMR-derived Q^n_{Si} populations (Table 3) reveal higher (≈0.55) and lower (≈0.41) x^3_{Si} and x^2_{Si} fractions, respectively; those NMR spectra further comprise weak signals from Q^4_{Si} and Q^1_{Si} tetrahedra ($x^n_{Si} \lesssim 0.02$).

From each set $\{x^n_{Si}\}$, we calculated the ^{29}Si NMR-derived value $\bar{N}^{Si}_{BO}(NMR_{Si})$, according to

$$\bar{N}^{Si}_{BO}(NMR_{Si}) = \sum_n n x^n_{Si} \quad (3)$$

Table 4 compares these results with their nominal counterparts $[\bar{N}^{Si}_{BO}(nom)]$, as well as those obtained by correcting the latter values for the observed non-negligible amounts of Q^1_P groups (whose presence releases Na^+/Ca^{2+} modifiers that become available for depolymerizing the silicate glass network), which provides a set of ^{31}P NMR-derived values, denoted $\{\bar{N}^{Si}_{BO}(NMR_P)\}$. Owing to the overall low amounts of P, each of $\bar{N}^{Si}_{BO}(NMR_P)$

Table 3. ^{29}Si NMR Results[a]

	net NMR peak			Q^1_{Si}			Q^2_{Si}			Q^3_{Si}			Q^4_{Si}				
label	$-\delta_{max}$ (ppm)	$-\delta_{CG}$ (ppm)	W (ppm)	$-\delta^1$ (ppm)	W^1 (ppm)	x^1	$-\delta^2$ (ppm)	W^2 (ppm)	x^2	$-\delta^3$ (ppm)	W^3 (ppm)	x^3	$-\delta^4$ (ppm)	W^4 (ppm)	x^4	$\bar{N}^{Si}_{BO}$(nom)	$\bar{N}^{Si}_{BO}(NMR_{Si})$
$BG_{2.6}(2.1)$	79.5	81.0	11.12	72.5	7.5	0.066	79.5	9.1	0.724	87.8	9.3	0.210	–	–	–	2.11	2.14
$BG_{6.0}(2.1)$	80.9	81.7	13.66	73.4	7.1	0.056	80.2	9.2	0.658	87.5	11.0	0.286	–	–	–	2.15	2.20
$BG_0(2.5)$	83.0	85.3	15.68	72.5	7.0	0.015	80.9	8.9	0.409	88.5	11.5	0.555	100.5	11.0	0.021	2.50	2.58
$BG_{1.0}(2.5)$	82.1	84.0	15.12	72.4	7.0	0.017	80.5	9.1	0.455	88.0	11.5	0.512	100.5	11.0	0.016	2.50	2.53
$BG_{2.0}(2.5)$	82.9	85.1	15.80	71.8	7.0	0.012	80.6	8.9	0.405	88.2	11.5	0.563	100.5	11.0	0.020	2.50	2.59
$BG_{4.0}(2.5)$	84.0	85.6	15.83	71.6	7.0	0.010	80.8	8.9	0.372	88.5	11.5	0.598	100.5	11.0	0.020	2.50	2.63
$BG_{6.0}(2.5)$	82.8	85.0	15.75	71.9	7.0	0.010	80.7	9.0	0.423	88.3	11.5	0.551	100.5	11.0	0.016	2.50	2.57
$BG_{2.6}(2.7)$	88.2	87.6	15.56	72.3	5.2	0.006	81.0	8.4	0.242	88.9	11.0	0.677	98.1	12.0	0.075	2.74	2.82
$BG_0(2.9)$	89.8	90.1	14.70	–	–	–	80.9	8.2	0.094	89.9	12.5	0.793	101.7	12.8	0.113	2.93	3.02
$BG_{2.0}(2.9)$	89.9	90.1	14.57	–	–	–	81.0	8.2	0.108	89.9	12.4	0.791	101.6	12.5	0.101	2.93	2.99
$BG_{3.0}(2.9)$	89.2	89.0	15.53	–	–	–	80.9	8.4	0.144	89.3	12.5	0.779	101.4	12.9	0.077	2.93	2.93
$BG_{4.0}(2.9)$	89.7	89.9	14.46	–	–	–	81.0	8.1	0.118	89.7	12.5	0.791	101.7	12.7	0.091	2.93	2.97
$BG_{6.0}(2.9)$	90.0	90.1	14.41	–	–	–	80.8	8.1	0.121	90.0	12.2	0.778	101.7	12.6	0.101	2.93	2.98

[a]The data involve the peak maximum (δ_{max}; uncertainty ±0.2 ppm), the center-of-gravity shift (δ_{CG}; ±0.3 ppm) and the fwhm height (W; ±0.3 ppm) of the net ^{29}Si NMR signal, and the chemical shift (δ^n), fwhm height (W^n), and fractional population (x^n) of each Q^n_{Si} peak contribution resulting from spectral deconvolution. $\bar{N}^{Si}_{BO}$(nom) and $\bar{N}^{Si}_{BO}(NMR_{Si})$ represent the silicate network connectivity obtained from the BG composition and by eq 3, respectively.

dx.doi.org/10.1021/jp409652k | J. Phys. Chem. B 2014, 118, 833–844

Table 4. Fractional populations of Q^n_{Si} Groups derived by MD simulations and NMR[a]

label	x^n_P populations[b]		x^n_{Si} populations[b]				silicate network connectivity			
	Q^0_P	Q^1_P	Q^1_{Si}	Q^2_{Si}	Q^3_{Si}	Q^4_{Si}	$\bar{N}^{Si}_{BO}$(nom)	$\bar{N}^{Si}_{BO}(NMR_P)$[c]	$\bar{N}^{Si}_{BO}(NMR_{Si})$[d]	$\bar{N}^{Si}_{BO}(MD)$[e]
$BG_{2.6}(2.1)$	0.834 (0.959)	0.166 (0.041)	0.186 (0.066)	0.517 (0.724)	0.266 (0.210)	0.021 (0.000)	2.11	2.11	2.14	2.10
$BG_{6.0}(2.1)$	0.798 (0.955)	0.200 (0.045)	0.197 (0.056)	0.514 (0.658)	0.252 (0.286)	0.027 (0.000)	2.15	2.14	2.20	2.09
$BG_0(2.5)$	–	–	0.068 (0.015)	0.428 (0.409)	0.425 (0.555)	0.076 (0.021)	2.50	2.50	2.58	2.50
$BG_{1.0}(2.5)$	0.670 (0.899)	0.318 (0.101)	0.073 (0.017)	0.426 (0.455)	0.435 (0.512)	0.065 (0.016)	2.50	2.50	2.53	2.49
$BG_{2.0}(2.5)$	0.721 (0.896)	0.267 (0.104)	0.080 (0.012)	0.418 (0.405)	0.440 (0.563)	0.060 (0.020)	2.50	2.50	2.59	2.48
$BG_{4.0}(2.5)$	0.622 (0.931)	0.364 (0.069)	0.084 (0.010)	0.443 (0.372)	0.409 (0.598)	0.063 (0.020)	2.50	2.49	2.63	2.45
$BG_{6.0}(2.5)$	0.690 (0.902)	0.304 (0.098)	0.087 (0.010)	0.457 (0.423)	0.392 (0.551)	0.062 (0.016)	2.50	2.48	2.57	2.42
$BG_{2.6}(2.7)$	0.517 (0.838)	0.475 (0.162)	0.041 (0.006)	0.336 (0.242)	0.507 (0.677)	0.115 (0.075)	2.74	2.73	2.82	2.70
$BG_0(2.9)$	–	–	0.016 (0.000)	0.225 (0.094)	0.571 (0.793)	0.189 (0.113)	2.93	2.93	3.02	2.93
$BG_{2.0}(2.9)$	0.417 (0.795)	0.553 (0.205)	0.017 (0.000)	0.246 (0.108)	0.553 (0.791)	0.183 (0.101)	2.93	2.92	2.99	2.90
$BG_{3.0}(2.9)$	0.444 (0.814)	0.528 (0.186)	0.020 (0.000)	0.252 (0.144)	0.562 (0.779)	0.166 (0.077)	2.93	2.91	2.93	2.87
$BG_{4.0}(2.9)$	0.440 (0.805)	0.554 (0.195)	0.022 (0.000)	0.269 (0.118)	0.539 (0.791)	0.169 (0.091)	2.93	2.90	2.97	2.86
$BG_{6.0}(2.9)$	0.460 (0.821)	0.527 (0.179)	0.028 (0.000)	0.295 (0.121)	0.529 (0.778)	0.149 (0.101)	2.93	2.89	2.98	2.79

[a]Values within parentheses correspond to the populations obtained by NMR. Typical standard deviations of the MD-generated x^n_P and x^n_{Si} populations are $\sigma = 0.034$ and $\sigma = 0.011$, respectively, as estimated from all simulations that involved ≈6000 atoms (see the Supporting Information). [b]The MD-derived structures also comprise minor amounts of Q^2_P ($x^2_P \lesssim 0.03$) and Q^0_{Si} ($x^0_{Si} \lesssim 0.01$) groups that are not listed. [c]Corrected for the NMR-derived minor Q^1_P contributions. [d]Obtained from the ^{29}Si NMR-derived $\{x^n_{Si}\}$ sets via eq 3. [e]Obtained from the MD data.

remains close to its $\bar{N}^{Si}_{BO}$(nom) analogue (within ≤1% deviation throughout). Whereas the $\bar{N}^{Si}_{BO}(NMR_{Si})$ values stay fairly constant across each BG(2.5) and BG(2.9) branch, they are consistently 2−4% larger than their *nominal* counterparts. Yet, it is gratifying that the deviations between the respective $\bar{N}^{Si}_{BO}$ data obtained by ^{31}P and ^{29}Si NMR typically only amount to ≈3%, with the largest discrepancy (≈5%) observed for the $BG_{4.0}(2.5)$ glass.

4.3. Silicate and Phosphate Speciations: MD Simulations versus NMR. Here, we present the MD-modeled $\{Q^n_{Si}\}$ and $\{Q^n_P\}$ speciations and contrast their predictions with the experimental data obtained by MAS NMR.

4.3.1. NBO Distribution among Phosphate Groups. Some of the sparse experimental reports on (semi)quantitative $\{x^0_P, x^1_P\}$ populations of $Na_2O-CaO-SiO_2-P_2O_5$ structures concluded that the Q^1_P groups generally increase with the P_2O_5 content.[16,26,32] In contrast, Grussaute et al.[31] reported that the Q^1_P populations are independent thereof, at least for $x(P_2O_5) \leq$ 2.4 mol % and high silicate network connectivities (2.65−3.0). However, inspection of their ^{31}P NMR data reveals a clear growth of x^1_P when $\bar{N}^{Si}_{BO}$ increases, but this trend was not commented. Mercier et al.[32] highlighted a dependence of the Q^1_P fraction on the SiO_2 content of the glass, further inferring that it increased concomitantly with the silicate network polymerization; yet, their glass-series design did not allow for reaching a quantitative $x^1_P/\bar{N}^{Si}_{BO}$ correlation. Such a relationship is established herein.

Table 4 lists the sets of MD-generated $\{x^0_P, x^1_P\}$ populations for the present structures. It is gratifying that the following qualitative trends fully accord with the experimental results of section 3.1: (i) The Q^1_P population grows steadily as $\bar{N}^{Si}_{BO}$ increases, with the extreme values of x^1_P =0.17 and x^1_P ≈0.55 observed for the $BG_{2.6}(2.1)$ and BG(2.9) structures, respectively. (ii) At a fixed silicate network connectivity, the Q^1_P population remains essentially constant when the P content varies (Table 4). The primary discrepancy between the $\{x^n_P\}$ sets obtained from ^{31}P NMR and the MD calculations is the significantly lower orthophosphate populations in the modeled structures, whereas the Q^1_P contributions are consistently 2.5−3 times higher than their experimental counterparts. Noteworthy, the deviations constitute a straightforward scaling, essentially independent of the $\bar{N}^{Si}_{BO}$ value. Previous MD studies of the $Na_2O-CaO-SiO_2-P_2O_5$ system have focused almost exclusively on the "45S5" composition [i.e., $BG_{2.6}(2.1)$], where consistently higher x^1_P values were observed[17,18,44−46,49,50] compared to those (≈0) estimated by ^{31}P NMR.[24,30,43] This discrepancy likely reflects slight x^1_P overestimations in MD simulations, and a corresponding potential underestimation by ^{31}P MAS NMR whenever the Q^1_P population is at the detection level of the technique, such as for 45S5 (see the Supporting Information). The present MD-generated phosphate speciation of $BG_{2.6}(2.1)$ confirm previously modeled results on 45S5,[17,18,46,49,50] while our remaining specimens complement the very few MD reports from other Na−Ca−Si−P−O compositions[17,18] by systematically exploring a significantly wider compositional range than previously considered.

Because the NMR-derived phosphate speciations solely comprise Q^0_P and Q^1_P groups, there is a direct mapping between x^1_P and $\bar{N}^P_{BO}$ (i.e., the average number of BO atoms per PO_4 tetrahedron), whereas the modeled counterparts additionally comprise minor x^2_P populations ($\lesssim$0.03; see the Supporting Information). To gain quantitative insight into the relationship between the Q^1_P population and the silicate network polymerization, being of direct concern for designing BG specimens

dx.doi.org/10.1021/jp409652k | J. Phys. Chem. B 2014, 118, 833−844

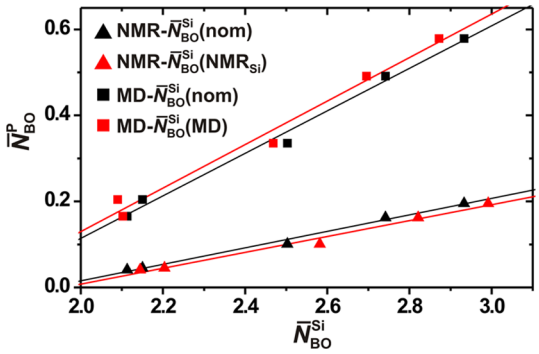

Figure 4. Average number of BO atoms at the phosphate groups ($\bar{N}^{P}_{BO}$) in the BG structures, plotted against its Si analogue ($\bar{N}^{Si}_{BO}$), as obtained either by ^{29}Si NMR experiments [$\bar{N}^{Si}_{BO}$(NMR$_{Si}$)], or by MD simulations [$\bar{N}^{Si}_{BO}$(MD)]. Averages were taken over all $\bar{N}^{P}_{BO}$-values within each series of constant $\bar{N}^{Si}_{BO}$(nom). Given that the experimental and modeled $\bar{N}^{Si}_{BO}$ values generally differ slightly from their nominal counterparts [$\bar{N}^{Si}_{BO}$(nom)], the results of correlating the {$\bar{N}^{P}_{BO}$(NMR)} and {$\bar{N}^{P}_{BO}$(MD)} set with $\bar{N}^{Si}_{BO}$(nom) are also provided (red symbols). Straight lines represent best-fit results of each $\bar{N}^{P}_{BO}/\bar{N}^{Si}_{BO}$ correlation and method {MD-$\bar{N}^{Si}_{BO}$(nom), MD-$\bar{N}^{Si}_{BO}$(MD), NMR-$\bar{N}^{Si}_{BO}$(nom), NMR-$\bar{N}^{Si}_{BO}$(NMR$_{Si}$)}; they are associated with the respective R^2 correlation coefficients of {0.988, 0.977, 0.989, 0.981}.

with optimal bioactivity, we fitted the {$\bar{N}^{P}_{BO}$} set against {$\bar{N}^{Si}_{BO}$}. For both the NMR and MD generated data, Figure 4 reveals an approximately linear relationship over the present parameter space {$2.1 \le \bar{N}^{Si}_{BO} \le 2.9$; $p \le 6.0$}. This trend persists regardless of whether each NMR/MD derived set {$\bar{N}^{P}_{BO}$} is correlated with the composition-dictated $\bar{N}^{Si}_{BO}$(nom) values, or with those obtained from either of ^{29}Si NMR [$\bar{N}^{Si}_{BO}$(NMR$_{Si}$)] or MD simulations [$\bar{N}^{Si}_{BO}$(MD)] (the latter are discussed below). As phase separation tendencies were observed for the BG$_{6.0}$(2.9) glass (see section 3.1), the linear $\bar{N}^{P}_{BO}/\bar{N}^{Si}_{BO}$ correlation likely breaks down for higher values of $\bar{N}^{Si}_{BO}$ and/or x(P$_2$O$_5$).

4.3.2. NBO Distribution among Silicate Groups. We now focus on the BO/NBO partitioning among the network-forming SiO$_4$ groups, i.e., the *n*-distribution of {Q^n_{Si}}. The MD-derived {Q^n_{Si}} speciations are contrasted with their experimental counterparts in Table 4. As required and also in full accordance with ^{29}Si NMR, the modeled structures manifest essentially equal {Q^n_{Si}} sets within each glass family of constant $\bar{N}^{Si}_{BO}$(nom)-value (regardless of the P content), whereas the Q^n_{Si} distribution shifts progressively toward higher *n* for increasing silicate network polymerization. For each silicate network, its average number of BO atoms, $\bar{N}^{Si}_{BO}$(MD), was calculated according to eq 3. The {$\bar{N}^{Si}_{BO}$(MD)} set accords well with its nominal {$\bar{N}^{Si}_{BO}$(nom)} counterpart, besides a slight but consistent decrease of the MD-generated results when the P content increases; this is readily explained by the presence of significant fractions of Q^1_P groups that release some Na^+/Ca^{2+} cations relative to the as-assumed scenario of solely orthophosphate species when the present glass compositions were devised (see section 2). However, owing to the overall low P$_2$O$_5$ contents (≤6 mol %), the observed reduction of $\bar{N}^{Si}_{BO}$ remains very minor.

The major distinction between the experimental and modeled data is the significantly wider {Q^n_{Si}} distributions observed from the latter (Table 4). The NMR/MD derived {Q^n_{Si}} sets are displayed in Figure 5, which also includes results by assuming either a "binary" or "random" (statistical) BO/NBO distribution among the SiO$_4$ groups. The ^{29}Si NMR-derived silicate speciation generally comprises three terms,

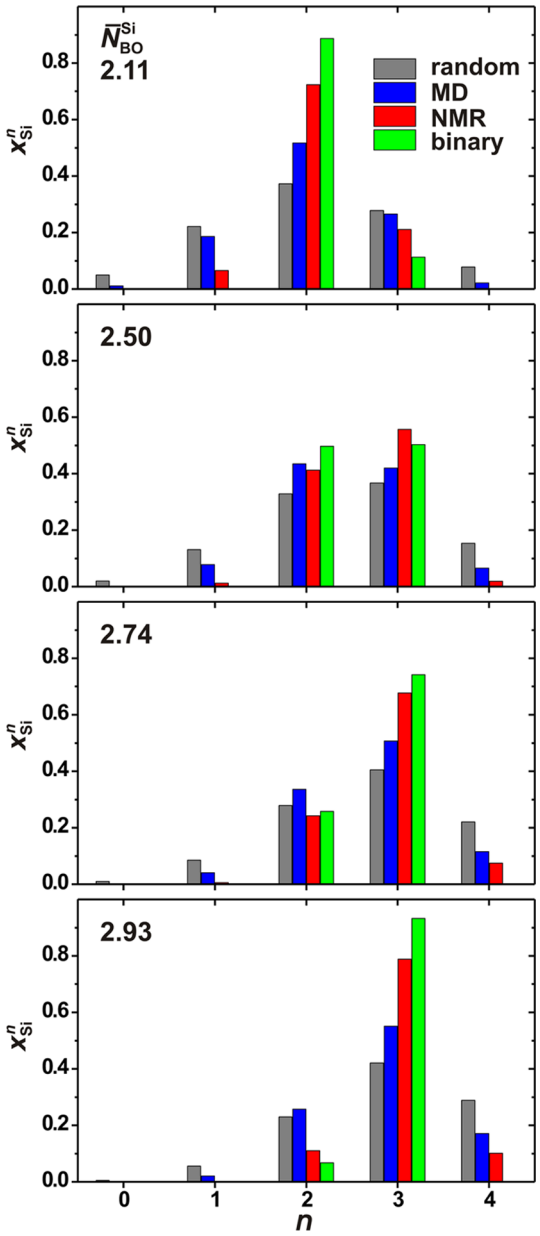

Figure 5. Q^n_{Si} fractional populations determined either by ^{29}Si NMR or MD simulations and plotted versus the number of BO atoms (*n*) at the SiO$_4$ group. For the glass series BG(2.5) and BG(2.9) that comprise several samples, the {x^n_{Si}} values represent averages over all members within the series. The results are compared with the predictions from binary and random NBO/BO distributions (calculated from the expressions of ref 21) for each as-indicated $\bar{N}^{Si}_{BO}$(nom) value.

{Q^{n-1}_{Si}, Q^n_{Si}, Q^{n+1}_{Si}}, in agreement with some recent NMR reports on BGs,[30,32,33] although earlier studies generally employed spectra deconvolutions into two signals.[16,24,27,43] The modeled/experimental {Q^n_{Si}} populations and the binary/random distribution scenarios are next compared by their respective distribution *widths* σ. As very similar σ-values are observed among the various glass structures for a given distribution type ("NMR/MD/random"; except for the binary scenario that anyway obeys $\sigma \le 0.5$), only averages over the entire set of samples are considered, which compare as follows:

$$\sigma_{binary}(\approx 0.4) < \sigma_{NMR}(0.52) < \sigma_{MD}(0.73) < \sigma_{random}(0.95) \quad (4)$$

dx.doi.org/10.1021/jp409652k | J. Phys. Chem. B 2014, 118, 833−844

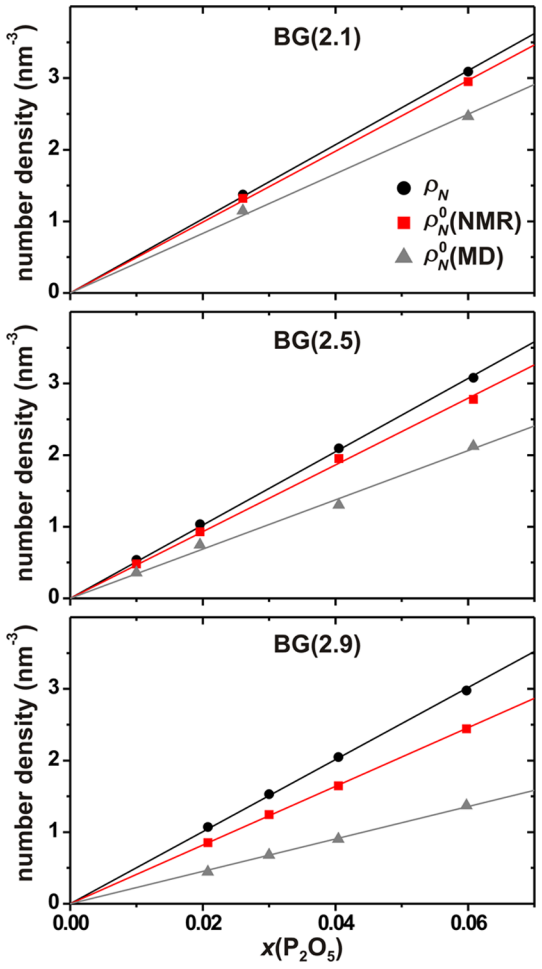

Figure 6. Number density (number of species per nm^3) of P atoms (ρ_N) and orthophosphate groups (ρ_N^0), plotted against the molar fraction of P_2O_5 for the as-indicated BG($\bar{N}_{BO}^{Si}$) series of glasses. ρ_N was obtained from the stoichiometric glass composition and its accompanying experimental density ρ (see Table 1), whereas $\rho_N^0 = x_P^0\rho_N$ involves the fractional population x_P^0 obtained either by ^{31}P NMR or by MD simulations. Straight lines represent best-fit results.

with their (approximate) values given within parentheses.

We conclude that the experimentally determined $\{x_{Si}^n\}$ sets, typically comprising three (significant) contributions, is slightly wider than a binary *n*-distribution, whereas the MD-derived counterpart is intermediate between the two limiting models, meaning that it is significantly wider than the scenarios of either a binary distribution or that estimated by NMR, but markedly more ordered than predicted from a statistical BO/NBO partitioning among the SiO_4 groups.

5. DISCUSSION

5.1. Orthophosphate Content versus Silicate Network Connectivity. For a wide range of $Na_2O-CaO-SiO_2-P_2O_5$ glass compositions, the present experimental and modeling results (Table 4) firmly establish and extend the inferences by Grussaute et al.[31] that for a constant network polymerization, the Q_P^1 population is independent of the P_2O_5 content of the glass (provided that y(CaO) is fixed[31]). Hence, the total orthophosphate population [n_P^0; see eq 1] is directly proportional to the net stoichiometric amount of P in the structure, as evidenced by Figure 6 that plots each experimental and modeled *number density*, ρ_N and ρ_N^0 of the P atoms and the Q_P^0 species, respectively, against the P_2O_5 content of the glass. Two important inferences may be made, both having bearings on future BG glass design:

(i) Considering previous demonstrations that the bioactivity increases with the P content of the BG,[6,7,9,22] our present results evidence a direct correlation between the bioactivity and the *ortho*phosphate content of the structure. Further, from the direct n_P/bioactivity correlation inferred in refs 15 and 22 follows that the bioactivity increases *monotonically* with n_P^0 [see eq 1], thereby establishing the validity of hypothesis **B** in section 2.

(ii) One may readily design a BG$_p$($\bar{N}_{BO}^{Si}$) composition that combines a favorable silicate network polymerization with a high P content, at least for $p \leq 6.0$. Hence, for the range of suitable silicate network connectivities $2.0 \lesssim \bar{N}_{BO}^{Si} \lesssim 2.6$ (discussed further in section 5.2), an optimal bioactivity is attained by arranging the highest possible P content, without altering the $\bar{N}_{BO}^{Si}$-value significantly, as the majority of the phosphate species are not forming bonds to other SiO_4 or PO_4 groups, but enter the structure as isolated orthophosphate ions (provided that the glass modifier content is increased accordingly; see section 2 and Table 1).

5.2. Bioactivity versus Silicate Network Connectivity. Early work concluded that a *bioactive* glass composition required a "network connectivity <3".[11,12] This originated from the incorrect assumption of a nonpreferential BO/NBO distribution among Si and P; because P is mainly present as orthophosphate ions, their Na^+/Ca^{2+} consumption then leads to a higher than predicted $\bar{N}_{BO}^{Si}$-value; to avoid such confusions, we refer specifically to the *silicate* network connectivity, i.e., $\bar{N}_{BO}^{Si}$.[15] Yet, the precise $\bar{N}_{BO}^{Si}$-range that optimizes the bioactivity remains unsettled in the current absence of a systematic investigation.

On the basis of published data from a large series of $Na_2O-CaO-SiO_2-P_2O_5$ compositions,[6] we proposed $\bar{N}_{BO}^{Si} \lesssim 2.7$ as a *necessary* criterion for bioactivity, with *optimal* $\bar{N}_{BO}^{Si}$ values predicted at the upper range of 2.5–2.6, beyond which the bioactivity diminishes rapidly.[15] According to these predictions, the bioactivity increases from the BG(2.1) to the BG(2.5) glass branch—with the fastest HCA growth expected from the $BG_{6.0}$(2.5) specimen due to its highest P content—whereas $BG_{2.6}$(2.7) is anticipated to display a low bioactivity and no member of the BG(2.9) series should give physiological responses. While bioactivity testing is underway for the current glasses, the hypothesis that $\bar{N}_{BO}^{Si} \approx 2.55$ provides optimum conditions is supported further by the very recent work of Duée et al.[9] They employed "mixture designs" to identify optimal BG candidates with $x(P_2O_5) \leq 0.05$; it amounted in two "best" glass compositions, both incidentally exhibiting $\bar{N}_{BO}^{Si}$ = {2.56; 2.60}, despite that the silicate network connectivity was not a targeted parameter in their assessments. Noteworthy, the "D47" composition[9] ($0.215Na_2O-0.265CaO-0.470SiO_2-0.050P_2O_5$) is almost identical to a "$BG_{5.0}$(2.5)" glass in our nomenclature, i.e., $0.214Na_2O-0.278CaO-0.458SiO_2-0.050P_2O_5$. The onset of HCA formation from D47 was twice as rapid as for the "45S5 Bioglass",[9] hence providing further support for our stated optimal $\bar{N}_{BO}^{Si}$-range.

Another question is if the bioactivity-increase across the range $2.0 \lesssim \bar{N}_{BO}^{Si} \lesssim 2.6$ and its sharp reduction as $\bar{N}_{BO}^{Si}$ grows further can be rationalized from a structural viewpoint. The $\{Q_{Si}^n\}$ speciations of Table 3 reveal that the most bioactive glasses exhibit structures built primarily by Q_{Si}^2 and Q_{Si}^3 groups,

dx.doi.org/10.1021/jp409652k | J. Phys. Chem. B 2014, 118, 833–844

i.e., representing interconnected chain/ring motifs with a significant cross-linking: if the latter is negligible, then the BG degrades too rapidly in its contact with body fluids, thereby preventing significant HCA formation.[6,9] In contrast, a too high polymerization of the network impedes its degradability in solutions due to the large number of Si−O−Si bonds requiring hydrolysis, coupled with a diminished Na^+/Ca^{2+} reservoir and accompanying reduced ion dissolution associated with the (too) Si-rich composition. Apparently, the best compromise between these two limits occurs when the Q^2_{Si} and Q^3_{Si} populations are nearly matched, i.e., when $\bar{N}^{Si}_{BO} \approx 2.5$ (see Table 4), as opposed to the (perhaps more intuitive) scenario of $\bar{N}^{Si}_{BO} \approx 2.0$ that reveals predominantly Q^2_{Si} moieties. This is one reason why the link between the glass solubility and the bioactivity is not strict.

As the network polymerization increases across the range 2.1−2.9, the Q^3_{Si} population grows steadily at the expense of its Q^2_{Si} counterpart; while this effect alone cannot explain the nonmonotonic dependence of the bioactivity on $\bar{N}^{Si}_{BO}$, the bioactivity might reduce when Q^3_{Si} reaches above some "critical" level (≥70%, according to Table 3). Yet, the emergence of Q^4_{Si} structural groups is apparently a more accurate indicator for the onset of "non-bioactivity". While Q^4_{Si} motifs are essentially absent in the BG structures associated with $\bar{N}^{Si}_{BO} \leq 2.5$, their population increases steeply for more polymerized networks; they constitute ≈10% out of the total SiO_4 speciation for the nonbioactive BG(2.9) compositions (Table 3). The loss of bioactivity may be understood from the significantly higher cross-linking invoked by the Q^4_{Si} groups and the accompanying local depletion of glass modifier ions; altogether these features create structural portions that more strongly resists degradation in aqueous medium compared to the chain/sheet-like motifs prevailing in the *bioactive* glass structures. These inferences were made from the NMR-derived $\{Q^n_{Si}\}$ speciations; however, as in the case of the Q^1_P populations, this trend is also mirrored by the modeled structures (Table 4).

5.3. The Roles of Na and Ca. Once fixating both the P content and silicate network connectivity, the n_{Na}/n_{Ca} molar ratio constitutes the remaining free parameter for a given $Na_2O-CaO-SiO_2-P_2O_5$ glass formulation. Despite influencing the bioactivity to a lesser extent than the $\{\bar{N}^{Si}_{BO}, n_P\}$ pair, the relative Na/Ca content is worth discussing as its bearing on the bioactivity yet remains to be systematically assessed, particularly considering indications that the bioactivity-boost for increasing P content may be strictly monotonic only over a range of relative Na/Si amounts within $0.8 \lesssim n_{Na}/n_{Si} \lesssim 1.2$.[15]

Keeping either a large Na or Ca content has both its pros and cons. Large amounts of Ca are beneficial for primarily three reasons: (i) Being a component of HCA, higher dissolution rates of Ca improves the apatite supersaturation.[2,3,5] (ii) The $\{x^0_P, x^1_P\}$ values depend to some extent on the n_{Na}/n_{Ca} ratio, with the desirable orthophosphate fraction increasing concurrently with the Ca content.[31] (iii) Large amounts of Na^+ ions induces cytotoxicity.[9,51] In contrast, arranging a large Na content is favorable for (i) facilitating the preparation of P-rich glasses by lowering the melting temperature, and particularly, (ii) enhancing the glass solubility; the higher Na^+ mobility relative to Ca^{2+} overall accelerates the surface reactions and elevates the local pH, altogether stimulating the calcium phosphate formation.[2,3,5,29]

Noteworthy, as both the Ca^{2+} and PO_4^{3-} ions are dispersed throughout the glass matrix,[24−27] an increased glass degradation *also* facilitates their release (*vide infra*). We therefore hypothesize that a relatively high n_{Na}/n_{Ca} ratio within 1.0−2.0 (i.e., $0.3 \leq y(CaO) \leq 0.5$) may release an *otherwise stricter* lower bound on the $\bar{N}^{Si}_{BO}$-value, thereby allowing the combination of a high bioactivity with a relatively condensed silicate network exhibiting $\bar{N}^{Si}_{BO} \approx 2.5$ (see section 5.2). Furthermore, given that each Na^+ and Ca^{2+} species associate with both Si and P (section 4.1), altering the n_{Na}/n_{Ca} ratio offers a route to tune the glass−surface reactivity, and thereby the BG degradation, without any significant bearings on the $\bar{N}^{Si}_{BO}$-value. Note, however, that increasing the relative amount of Ca (i.e., decreasing n_{Na}/n_{Ca}) may be favorable as it elevates x^0_P *slightly*,[31] and thereby the net orthophosphate content [see eq 1].

5.4. Recommendations for Bioactivity Optimizations. The present results suggest that future bioactivity-composition assessments should target the parameter-triplet $\{\bar{N}^{Si}_{BO}, n_P, n_{Na}/n_{Ca}\}$ in the search for optimal BG compositions. Our suggested $\{\bar{N}^{Si}_{BO}, n_P, n_{Na}/n_{Ca}\}$ parametrization of the glass composition provides more transparent insight into the composition-bioactivity relationships compared with the standard formulations expressed as oxide equivalents. The bioactivity is mainly dictated by the $\{\bar{N}^{Si}_{BO}, n_P\}$ pair, and to a lesser extent by the exact n_{Na}/n_{Ca} ratio. Hence, it is expected to be optimized at the highest incorporable P_2O_5 content around the parameter space $\{\bar{N}^{Si}_{BO} \approx 2.55, 1 \lesssim n_{Na}/n_{Ca} \lesssim 2\}$.[15] The feasibility of preparing P-richer compositions than $x(P_2O_5) > 0.06$ needs to be tested. Future work must also more quantitatively define our suggested *weak* interdependence between these bioactivity descriptors. Additionally, the "optimal parameter-spaces" stated herein are strictly only applicable to Na−Ca−Si−P−O glasses (and limiting systems thereof), and their transferability to related M−M′−Si−P−O glasses remains to be explored.

6. CONCLUSIONS

The alterations of the Q^n_{Si} and Q^n_P speciations in a series of 13 glasses were for the first time explored systematically over a wide compositional range within the $Na_2O-CaO-SiO_2-P_2O_5$ system, by using a combination of atomistic MD simulations and $^{31}P/^{29}Si$ solid-state NMR experiments; both techniques generally revealed equivalent qualitative trends. Our glass series design allowed for an independent probing of the structural changes accompanying a variation in either the P content of the BG or its silicate network connectivity; the series encompassed both bioactive ($2.1 \leq \bar{N}^{Si}_{BO} \leq 2.5$) and nonbioactive glass compositions ($\bar{N}^{Si}_{BO} > 2.7$). When $\bar{N}^{Si}_{BO}$ increases from 2.1 to 2.9, both the MD/NMR-derived $\{Q^n_{Si}\}$ speciations reveal net $Q^2_{Si} \rightarrow Q^3_{Si}$ conversions (as expected). However, despite that the network polymerization increases accordingly throughout the entire range of *bioactive* glass compositions ($\bar{N}^{Si}_{BO} \lesssim 2.7$), the progressive formation of Q^3_{Si} groups itself does not obviously correlate with the transition from bioactive to nonbioactive compositions, which merely coincides with the emergence of non-negligible (≳10%) contributions of Q^4_{Si} groups; the accompanying markedly enhanced structural cross-linking from four BO atom per SiO_4 tetrahedron (as opposed to 1−3 BO) together with a local depletion of readily released Na^+/Ca^{2+} cations strongly diminishes the glass degradation in aqueous media.

If the silicate network connectivity of the BG remains constant, the $\{Q^0_P, Q^1_P\}$ fractional populations are independent of the amount of P_2O_5 (at least for $x(P_2O_5) \leq 0.06$), thereby providing a direct link between the orthophosphate content and n_P. In contrast, if n_P remains constant, the fraction of Q^0_P

dx.doi.org/10.1021/jp409652k | J. Phys. Chem. B 2014, 118, 833−844

species decreases linearly as $\bar{N}_{BO}^{Si}$ increases. Fortunately, for the network connectivity-range $2.0 \lesssim \bar{N}_{BO}^{Si} \lesssim 2.6$ that encompasses nearly all *bioactive* glass compositions, Q_P^0 moieties constitute $\gtrsim$80% of the total phosphate speciation, thereby rationalizing earlier statements[15,22] that the bioactivity increases monotonically with the P content of the BG (provided that the glass modifier reservoir is sufficiently large to charge-balance all Q_P^0 groups). By showing that the Q_P^0 concentration increases with the P_2O_5 molar fraction for a fixed silicate network connectivity, the present results prove it possible to design highly bioactive glasses that combine a favorable network connectivity with large amounts of readily released orthophosphate ions, thereby promoting both a rapid degradation of the glass network and a fast dissolution of biologically active ions.[52,53] The structural role of P is the key factor: the majority of all P species enter the structure as orthophosphate groups detached from the glass network; their fast dissolution enhances the bioactivity relative to a glass with the same network connectivity but a lower P content.

Future composition/bioactivity assessments/optimizations should target the parameter-set $\{\bar{N}_{BO}^{Si}, n_P, n_{Na}/n_{Ca}\}$. Each such triplet translates into a unique $Na_2O-CaO-SiO_2-P_2O_5$ glass composition, whose bioactivity may be *roughly* assessed by inspection, as each parameter influences the glass bioactivity in a predictable manner, while their effects may be tuned almost independently from each other. However, future studies must better quantify the expectedly weak correlation between the $\{x_P^0, x_P^1\}$ populations and the n_{Na}/n_{Ca} ratio,[31] as well as exploring the degree of correlation between the *bioactivity* of the glass and its *solubility*. As the latter may be changed by varying either the silicate network connectivity or the Na content of the BG, whose effects are likely synergetic, the $\bar{N}_{BO}^{Si}$-range providing high bioactivities is presumably not completely decoupled from the n_{Na}/n_{Ca} ratio: rather, we suggest that the increased solubility associated with Na-rich BGs may (slightly) alter the $\bar{N}_{BO}^{Si}$-values defining each transition between high/low/nonbioactive compositions. These ideas are currently being explored.

■ ASSOCIATED CONTENT

Supporting Information

Further information about the NMR spectra and the deconvolution procedures, discussion about the detection of Q_P^1 groups by ^{31}P NMR, as well as additional MD data and discussions thereof. This material is available free of charge via the Internet at http://pubs.acs.org.

■ AUTHOR INFORMATION

Corresponding Author

*E-mail: mattias.eden@mmk.su.se. Fax: +46 8 152187. Telephone: +46 8 162375.

Notes

The authors declare no competing financial interest.

■ ACKNOWLEDGMENTS

This work was supported by the Swedish Research Council (contract 2010-4943) and the Faculty of Sciences at Stockholm University. A.T. acknowledges support (University Research Fellowship) from the U.K.'s Royal Society. NMR equipment Grants from the Swedish Research Council, and the Knut and Alice Wallenberg Foundation are gratefully acknowledged. We thank Shahriar Iftekhar and Kirill Okhotnikov for their initial help and input regarding glass synthesis and MD simulations, respectively.

■ REFERENCES

(1) Hench, L. L.; Splinter, R. J.; Allen, W. C.; Greenlee, T. K. Bonding Mechanisms at the Interface of Ceramic Prosthetic Materials. *J. Biomed. Mater. Res.* **1971**, *2*, 117−141.
(2) Hench, L. L. Bioceramics−from Concept to Clinic. *J. Am. Ceram. Soc.* **1991**, *74*, 1487−1510.
(3) Jones, J. R. Review of Bioactive Glass: From Hench to Hybrids. *Acta Biomater.* **2013**, *9*, 4457−4486.
(4) Hench, L. L.; Polak, J. M. Third-Generation Biomedical Materials. *Science* **2002**, *295*, 1014−1017.
(5) Andersson, Ö. H.; Karlsson, K. H. On the Bioactivity of Silicate Glass. *J. Non-Cryst. Solids* **1991**, *129*, 145−151.
(6) Lebecq, I.; Désanglois, F.; Leriche, A.; Follet-Houttemane, C. Compositional Dependence on the *In Vitro* Bioactivity of Invert or Conventional Bioglasses in the Si-Ca-Na-P System. *J. Biomed. Mater. Res. A* **2007**, *83*, 156−168.
(7) O'Donnell, M. D.; Watts, S. J.; Hill, R. G.; Law, R. V. The Effect of Phosphate Content on the Bioactivity of Soda-Lime-Phosphosilicate Glasses. *J. Mater. Sci: Mater. Med.* **2009**, *20*, 1611−1618.
(8) Watts, S. J.; Hill, R. G.; O'Donnell, M. D.; Law, R. V. Influence of Magnesia on the Structure and Properties of Bioactive Glasses. *J. Non-Cryst. Solids* **2010**, *356*, 517−524.
(9) Duée, C.; Grattepanche-Lebecq, I.; Désanglois, F.; Follet-Houttemane, C.; Chai, F.; Hildebrand, H. F. Predicting Bioactive Properties of Phosphosilicate Glasses Using Mixture Designs. *J. Non-Cryst. Solids* **2013**, *362*, 47−55.
(10) Christie, J. K.; Tilocca, A. Molecular Dynamics Simulations and Structural Descriptors of Radioisotope Glass Vectors for *in Situ* Radiotherapy. *J. Phys. Chem. B* **2012**, *116*, 12614−12620.
(11) Strnad, Z. Role of the Glass Phase in Bioactive Glass-Ceramics. *Biomaterials* **1992**, *13*, 317−321.
(12) Hill, R. An Alternative View of the Degradation of Bioglass. *J. Mater. Sci. Lett* **1996**, *15*, 1122−1125.
(13) Stevels, J. M. Neue Erkenntnisse Uber Die Struktur Des Glases. *Philips Techn. Rdsch* **1960**, *9/10*, 337−349.
(14) O'Donnell, M. D.; Watts, S. J.; Law, R. V.; Hill, R. G. Effect of P_2O_5 Content in Two Series of Soda Lime Phosphosilicate Glasses on Structure and Properties - Part I: NMR. *J. Non-Cryst. Solids* **2008**, *354*, 3554−3560.
(15) Edén, M. The Split Network Analysis for Exploring Composition-Structure Correlations in Multi-Component Glasses: I. Rationalizing Bioactivity-Composition Trends of Bioglasses. *J. Non-Cryst. Solids* **2011**, *357*, 1595−1602.
(16) Elgayar, I.; Aliev, A. E.; Boccaccini, A. R.; Hill, R. G. Structural Analysis of Bioactive Glasses. *J. Non-Cryst. Solids* **2005**, *351*, 173−183.
(17) Tilocca, A.; Cormack, A. N. Structural Effects of Phosphorus Inclusion in Bioactive Silicate Glasses. *J. Phys. Chem. B* **2007**, *111*, 14256−14264.
(18) Tilocca, A.; Cormack, A. N.; de Leeuw, N. H. The Structure of Bioactive Silicate Glasses: New Insight from Molecular Dynamics Simulations. *Chem. Mater.* **2007**, *19*, 95−103.
(19) Tilocca, A. Structural Models of Bioactive Glasses from Molecular Dynamics Simulations. *Proc. R. Soc. A* **2009**, *465*, 1003−1027.
(20) Gunawidjaja, P. N.; Lo, A. Y. H.; Izquierdo-Barba, I.; García, A.; Arcos, D.; Stevensson, B.; Grins, J.; Vallet-Regí, M.; Edén, M. Biomimetic Apatite Mineralization Mechanisms of Mesoporous Bioactive Glasses as Probed by Multinuclear ^{31}P, ^{29}Si, ^{23}Na and ^{13}C Solid-State NMR. *J. Phys. Chem. C* **2010**, *114*, 19345−19356.
(21) Edén, M.; Sundberg, P.; Stålhandske, C. The Split Network Analysis for Exploring Composition-Structure Correlations in Multi-Component Glasses: II. Multinuclear NMR Studies of Alumino-Borosilicates and Glass-Wool Fibers. *J. Non-Cryst. Solids* **2011**, *357*, 1587−1594.

(22) Hill, R. G.; Brauer, D. S. Predicting the Bioactivity of Glasses Using the Network Connectivity or Split Network Models. *J. Non-Cryst. Solids* **2011**, *357*, 3884−3887.
(23) Gunawidjaja, P. N.; Mathew, R.; Lo, A. Y. H.; Izquierdo-Barba, I.; García, A.; Arcos, D.; Vallet-Regí, M.; Edén, M. Local Structures of Mesoporous Bioactive Glasses and Their Surface Alterations *In Vitro*: Inferences from Solid-State Nuclear Magnetic Resonance. *Philos. Trans. R. Soc. A* **2012**, *370*, 1376−1399.
(24) Martin, R. A.; Twyman, H. L.; Rees, G. J.; Smith, J. M.; Barney, E. R.; Smith, M. E.; Hanna, J. V.; Newport, R. J. A Structural Investigation of the Alkali Metal Site Distribution within Bioactive Glass Using Neutron Diffraction and Multinuclear Solid State NMR. *Phys. Chem. Chem. Phys.* **2012**, *14*, 12105−12113.
(25) Mathew, R.; Turdean-Ionescu, C.; Stevensson, B.; Izquierdo-Barba, I.; García, A.; Arcos, D.; Vallet-Regí, M.; Edén, M. Direct Probing of the Phosphate-Ion Distribution in Bioactive Silicate Glasses by Solid-State NMR: Evidence for Transitions between Random/Clustered Scenarios. *Chem. Mater.* **2013**, *25*, 1877−1885.
(26) Dupree, R.; Holland, D.; Mortuza, M. G.; Collins, J. A.; Lockyer, M. W. G. An MAS NMR Study of Network - Cation Coordination in Phosphosilicate Glasses. *J. Non-Cryst. Solids* **1988**, *106*, 403−407.
(27) Lockyer, M. W. G.; Holland, D.; Dupree, R. NMR Investigation of the Structure of some Bioactive and Related Glasses. *J. Non-Cryst. Solids* **1995**, *188*, 207−219.
(28) Ebisawa, Y.; Kokubo, T.; Ohura, K.; Yamamuro, T. Bioactivity of $CaO{\cdot}SiO_2$-Based Glasses: *In Vitro* Evaluation. *J. Mater. Sci: Mater. Med.* **1990**, *1*, 239−244.
(29) Karlsson, K. H.; Fröberg, K.; Ringbom, T. A Structural Approach to Bone Adhering of Bioactive Glasses. *J. Non-Cryst. Solids* **1989**, *112*, 69−72.
(30) Pedone, A.; Charpentier, T.; Malavasi, G.; Menziani, M. C. New Insights into the Atomic Structure of 45S5 Bioglass by Means of Solid-State NMR Spectroscopy and Accurate First-Principles Simulations. *Chem. Mater.* **2010**, *22*, 5644−5652.
(31) Grussaute, H.; Montagne, L.; Palavit, G.; Bernard, J. L. Phosphate Speciation in Na_2O-CaO-P_2O_5-SiO_2 and Na_2O-TiO_2-P_2O_5-SiO_2 Glasses. *J. Non-Cryst. Solids* **2000**, *263*, 312−317.
(32) Mercier, C.; Follet-Houttemane, C.; Pardini, A.; Revel, B. Influence of P_2O_5 Content on the Structure of SiO_2-Na_2O-CaO-P_2O_5 Bioglasses by ^{29}Si and ^{31}P MAS-NMR. *J. Non-Cryst. Solids* **2011**, *357*, 3901−3909.
(33) Fayon, F.; Duée, C.; Poumeyrol, T.; Allix, M.; Massiot, D. Evidence of Nanometric-Sized Phosphate Clusters in Bioactive Glasses as Revealed by Solid-State ^{31}P NMR. *J. Phys. Chem. C* **2013**, *117*, 2283−2288.
(34) Tilocca, A. Structure and Dynamics of Bioactive Phosphosilicate Glasses and Melts from *Ab Initio* Molecular Dynamics Simulations. *Phys. Rev. B* **2007**, *76*, 224202.
(35) Fujikura, K.; Karpukhina, N.; Kasuga, T.; Brauer, D. S.; Hill, R. G.; Law, R. V. Influence of Strontium Substitution on Structure and Crystallisation of Bioglass 45S5®. *J. Mater. Chem.* **2012**, *22*, 7395−7402.
(36) Tilocca, A. Models of Structure, Dynamics and Reactivity of Bioglasses: A Review. *J. Mater. Chem* **2010**, *20*, 6848−6858.
(37) Smith, W.; Forester, T. R. DL_POLY_2.0: A General-Purpose Parallel Molecular Dynamics Simulation Package. *J. Mol. Graphics* **1996**, *14*, 136−141.
(38) Todorov, I. T.; Smith, W.; Trachenko, K.; Dove, M. T. DL_POLY_3: New Dimensions in Molecular Dynamics Simulations via Massive Parallelism. *J. Mater. Chem.* **2006**, *16*, 1911−1918.
(39) Tilocca, A.; de Leeuw, N. H.; Cormack, A. N. Shell-Model Molecular Dynamics Calculations of Modified Silicate Glasses. *Phys. Rev. B* **2006**, *73*, 104209.
(40) MacKenzie, K. J. D.; Smith, M. E. *Multinuclear Solid-State NMR of Inorganic Materials*; Pergamon Press: Amsterdam, 2002.
(41) Leonova, E.; Izquierdo-Barba, I.; Arcos, D.; Lopez-Noriega, A.; Hedin, N.; Vallet-Regí, M.; Edén, M. Multinuclear Solid-State NMR Studies of Ordered Mesoporous Bioactive Glasses. *J. Phys. Chem. C* **2008**, *112*, 5552−5562.
(42) Mathew, R.; Gunawidjaja, P. N.; Izquierdo-Barba, I.; Jansson, K.; García, A.; Arcos, D.; Vallet-Regí, M.; Edén, M. Solid-State ^{31}P and ^{1}H NMR Investigations of Amorphous and Crystalline Calcium Phosphates Grown Biomimetically from a Mesoporous Bioactive Glass. *J. Phys. Chem. C* **2011**, *115*, 20572−20582.
(43) FitzGerald, V.; Pickup, D. M.; Greenspan, D.; Sarkar, G.; Fitzgerald, J. J.; Wetherall, K. M.; Moss, R. M.; Jones, J. R.; Newport, R. J. A Neutron and X-Ray Diffraction Study of Bioglass® with Reverse Monte Carlo Modelling. *Adv. Funct. Mater.* **2007**, *17*, 3746−3753.
(44) Xiang, Y.; Du, J. Effect of Strontium Substitution on the Structure of 45S5 Bioglasses. *Chem. Mater.* **2011**, *23*, 2703−2717.
(45) Du, J.; Xiang, Y. Effect of Strontium Substitution on the Structure, Ionic Diffusion and Dynamic Properties of 45S5 Bioactive Glasses. *J. Non-Cryst. Solids* **2012**, *358*, 1059−1071.
(46) Malavasi, G.; Pedone, A.; Menziani, M. C. Study of the Structural Role of Gallium and Aluminum in 45S5 Bioactive Glasses by Molecular Dynamics Simulations. *J. Phys. Chem. B* **2013**, *117*, 4142−4150.
(47) Murdoch, J. B.; Stebbins, J. F.; Carmichael, I. S. E. High-Resolution ^{29}Si NMR-Study of Silicate and Aluminosilicate Glasses - the Effect of Network-Modifying Cations. *Am. Mineral.* **1985**, *70*, 332−343.
(48) Maekawa, H.; Maekawa, T.; Kawamura, K.; Yokokawa, T. The Structural Groups of Alkali Silicate-Glasses Determined from ^{29}Si MAS-NMR. *J. Non-Cryst. Solids* **1991**, *127*, 53−64.
(49) Tilocca, A. Short- and Medium-Range Structure of Multicomponent Bioactive Glasses and Melts: An Assessment of the Performances of Shell-Model and Rigid-Ion Potentials. *J. Chem. Phys.* **2008**, *129*, 084504.
(50) Pedone, A.; Malavasi, G.; Menziani, M. C. Computational Insight into the Effect of CaO/MgO Substitution on the Structural Properties of Phospho-Silicate Bioactive Glasses. *J. Phys. Chem. C* **2009**, *113*, 15723−15730.
(51) Wallace, K. E.; Hill, R. G.; Pembroke, J. T.; Brown, C. J.; Hatton, P. V. Influence of Sodium Oxide Content on Bioactive Glass Properties. *J. Mater. Sci: Mater. Med.* **1999**, *10*, 697−701.
(52) Xynos, I. D.; Edgar, A. J.; Buttery, L. D. K.; Hench, L. L.; Polak, J. M. Gene-Expression Profiling of Human Osteoblasts Following Treatment with the Ionic Products of Bioglass 45S5 Dissolution. *J. Biomed. Mater. Res.* **2001**, *55*, 151−157.
(53) Tilocca, A.; Cormack, A. N. The Initial Stages of Bioglass Dissolution: A Car-Parrinello Molecular-Dynamics Study of the Glass-Water Interface. *Proc. R. Soc. A* **2011**, *467*, 2102−2111.